Applied Geochemistry 170 (2024) 106068

Contents lists available at ScienceDirect

Applied Geochemistry

journal homepage: www.elsevier.com/locate/apgeochem

Mineralogy and environmental stability of metallurgical slags from the Euronickel smelter, Vozarci, North Macedonia

Tamara Đorđević [a,b,*], Goran Tasev [c], Claudia Aicher [b], Anna Potysz [d], Peter Nagl [e], Christian L. Lengauer [b], Artur Pędziwiatr [f], Todor Serafimovski [c], Ivan Boev [c], Blažo Boev [c]

[a] Vienna University of Technology, E057-02 USTEM, Stadionallee 2, 1020, Vienna, Austria
[b] University of Vienna, Department of Mineralogy and Crystallography, Josef-Holaubek-Platz 2, 1090 Vienna, Austria
[c] Goce Delcev University, Faculty of Natural and Technical Sciences, Str. Goce Delčev 89, 2000, Stip, North Macedonia
[d] University of Wrocław, Faculty of Earth Sciences and Environmental Management, Institute of Geological Sciences, Pl. M. Borna 9, 50-204, Wrocław, Poland
[e] University of Vienna, Department of Lithospheric Research, Josef-Holaubek-Platz 2, 1090 Vienna, Austria
[f] Warsaw University of Life Sciences (WULS-SGGW), Institute of Agriculture, Department of Soil Science, Nowoursynowska Str. 159/37, 02–787 Warszawa, Poland

ARTICLE INFO

Editorial handling by: Dr V Ettler

Keywords:
Laterite Ni-Ore
Nickel smelting
Slag mineralogy
Weathering
Euronickel
Macedonia

ABSTRACT

The laterite Ni-smelting operations at Vozarci, Republic North Macedonia have produced large amounts of smelting wastes dumped in the close vicinity of the smelter. We examined phase composition and chemistry of the various types of slags (electric furnace slags, converter slag, magnetic slag) with the special focus on the phases containing potentially toxic elements in terms of their mineralogy, chemical composition, and responses to weathering. Electric furnace slags contain between 35 and 47 wt.% SiO_2, 21–40 wt.% Fe_2O_3, and 13–23 wt.% MgO; converter and magnetic slags are Fe-rich (76–77 wt.% of Fe_2O_3) with significant amounts of Ca (7.6–8.4 wt.% CaO) and S-portion (2–2.5 wt.% SO_3). All slags contain substantial amounts of the potentially toxic elements: Co (20–87 ppm), Cr (9600–17400 ppm), Ni (170–730 ppm), and Zn (150–380 ppm). Further mineralogical analyses showed that the slags consist of silicate glass, synthetic equivalents of olivines, orthopyroxenes, clinopyroxenes, and subordinate spinel-group phases, sulfides, and intermetallic compounds. Some of the slags had been subject to weathering since their dumping in 1982. The weathering results in the release of metals from primary slag phases, particularly from glass, and the partial immobilization of these metals in secondary soluble and insoluble minerals in the slag heaps (hydroxy-iron oxides, gypsum, anhydrite, syngenite, aphthitalite). The majority of slag samples exhibited increased leaching under conditions of lower pH (2.9) compared to higher pH (4.9). The contrast between leaching treatments was particularly evident for nickel (Ni), with leaching at a low pH of 2.9 reaching up to 135 times higher (MS) than at pH 4.9. At lower pH conditions, other contaminants of interest were leached out at a rate 4 to 76 times faster compared to the leaching achieved at pH 4.9, because they are the major source of potentially toxic elements.

1. Introduction

Pyrometallurgical slags are by-products of the metallurgy of either sulfide (e.g., Pb–Zn, Cu), oxide (e.g., Zn), or silicate (e.g., Ni) ores. The mining and smelting of metallic ores result in vast volumes of waste, comprising among others, slags, furnace ash, and industrial buildings. Slags resemble the silica melt formed during the pyrometallurgical recovery of the base metals by fusion in a blast furnace and are manufactured in huge amounts. Despite differences in the nature of the ores used for the metal production, their smelting leads to the formation of slags of similar phase-assemblages and composition. Typically, pyrometallurgical slags consist of silicate glass and silicate phases, synthetic analogues of pyroxene, melilite, olivine, spinel, sulfides and intermetallic compounds (Lottermoser, 2002; Piatak et al., 2015, 2021). Slags are often sources of potentially toxic elements (PTEs), especially Cr, Ni, Co, Cu, Zn, Pb, As and Sb, and continuously pose serious environmental risks in the areas where they are kept and to the surrounding ecosystems (Kierczak et al., 2009, 2021; Piatak et al., 2015 and references therein). The chemical composition and mineralogy of slag depend on the metallurgical processes that create the material and will influence its fate as waste material or as a reusable product (Ettler et al., 2009a,b; Warchulski, 2016). Furthermore, mineralogical studies on

* Corresponding author. E057-02 USTEM, Vienna University of Technology, Stadionallee 2, 1020, Vienna, Austria.
E-mail address: tamara.dordevic@tuwien.ac.at (T. Đorđević).

https://doi.org/10.1016/j.apgeochem.2024.106068
Received 14 December 2023; Received in revised form 7 May 2024; Accepted 6 June 2024
Available online 13 June 2024

slags are crucial for understanding the speciation of PTEs in primary solid phases and represent the first step in determining their environmental fate. Consequently, environmental studies on slags should focus on understanding the potential environmental impacts of slag deposited as waste, and concentrate on the geochemical and mineralogical properties of the material (Vitkova et al., 2010; Kierczak and Pietranik 2011; Jarošíková et al., 2017).

In today's World annual nickel (Ni) production, of up to 3 300 000 t of Ni as metal, comes from laterite or sulfide types of ores. At the beginning of the second decade of the XXI century only about 40 % of the Ni production came from laterites despite the fact that about 70 % of the ore reserves are found in this particular type of ore (Crundwell et al., 2011; Ettler et al., 2016). Currently, laterites are mostly used in ferro-nickel (FeNi) production, which finds its application in steelmaking industry. Curiously, smelting wastes from Ni production have only been analyzed at random in comparison to the waste materials from other smelting industries (Piatak et al., 2015, 2021). A few studies have investigated slags from smelting of sulfide Ni-ore (Gregurek et al., 1999; Lanteigne et al., 2012, 2014; Schindler, 2014); however, the geochemistry and mineralogy of slags from the Ni smelting using laterites have only been thoroughly studied a few times, by Kierczak et al. (2009), by Ettler et al. (2016, 2018) and by Ratié et al. (2016).

Euronickel Industries is a metallurgical company situated in Vozarci village, 7 km west of the town of Kavadarci in the Republic of North Macedonia, the primary wine-producing region in the country (Fig. 1a and b). This facility began operations in 1982 and, with a few minor interruptions, produces ferro-nickel alloy from lateritic nickel ores. The manufacturing process runs continuously 24 h a day, seven days a week. The smelting facility is spread across three sites (the smelter and two slag dumps, one near Vozarci village and the other near Šivec village) (Fig. 1a–d). The majority of the waste material (97 %) is slag from electric furnaces, with the residue coming from convertors. Aside from large amounts of fresh slag, much older slags were deposited in the area and have been exposed to atmospheric conditions for more than 40 years and are partly weathered. The vast majority of the slag material was firstly deposited on the slag dump near Vozarci village (at an area of 0.32 km^2, located 2.5 km south of the smelting facility; Fig. 1a–d), but since 2013, the produced slag has been deposited at the slag dump near Šivec village (at an area of 0.24 km^2), closer to the smelter (Fig. 1c). The height of the deposited slag material at both locations is approximately 20 m. Based on this information and well-known information about the specific gravity of materials (Saha and Sarker, 2016; Xi et al., 2018), we can estimate that approximately 20 400 000 t and 13 800 000 t of slag were deposited in the Vozarci and Šivec slag dumps, for a total of 34 200 000 t slag in both slag dumps.

Some environmental studies on the soils (Miceva et al., 2019), flying ashes (Boev et al., 2013; Bačeva Andonovska et al., 2015) and biota (Bačeva et al., 2012) in the vicinity of the Euronickel smelter have already been performed. Surprisingly, only limited information about the mineralogical and geochemical compositions of the waste materials from the slag dump and adjacent soils is publicly available. Only few conference contributions and papers in non-peer reviewed journals have been published in connection with the mineralogy of these slags and pre-reduced materials (Boev and Bermanec, 2005 and references therein).

Due to the deficit of the previous studies, considering both Euronickel slags, as well as the FeNi slags from lateritic Ni ores (produced formerly by Fe-Ni industry and at the moment by the Euronickel), the current paper provides new insights into the solid speciation of PTEs and their leaching, using examples of slags from both current smelting operation, as well as from past smelting operations near the city of Kavadarci in the Republic of North Macedonia.

2. Materials and methods

2.1. Smelting site history

Waste dumps of the pyrometallurgical plant Euronickel Industries that produces ferronickel (FeNi) are located on the outskirts of the Vozarci village area and nearby city of Kavadarci, Republic North Macedonia (Fig. 1a and b). This facility, initially named Feni (derived from ferro-nickel), was put into operation for the first time in 1982 and it was closely related with nickel-bearing ore production from the Ržanovo mine, located 40 km away in southwestern from the smelting

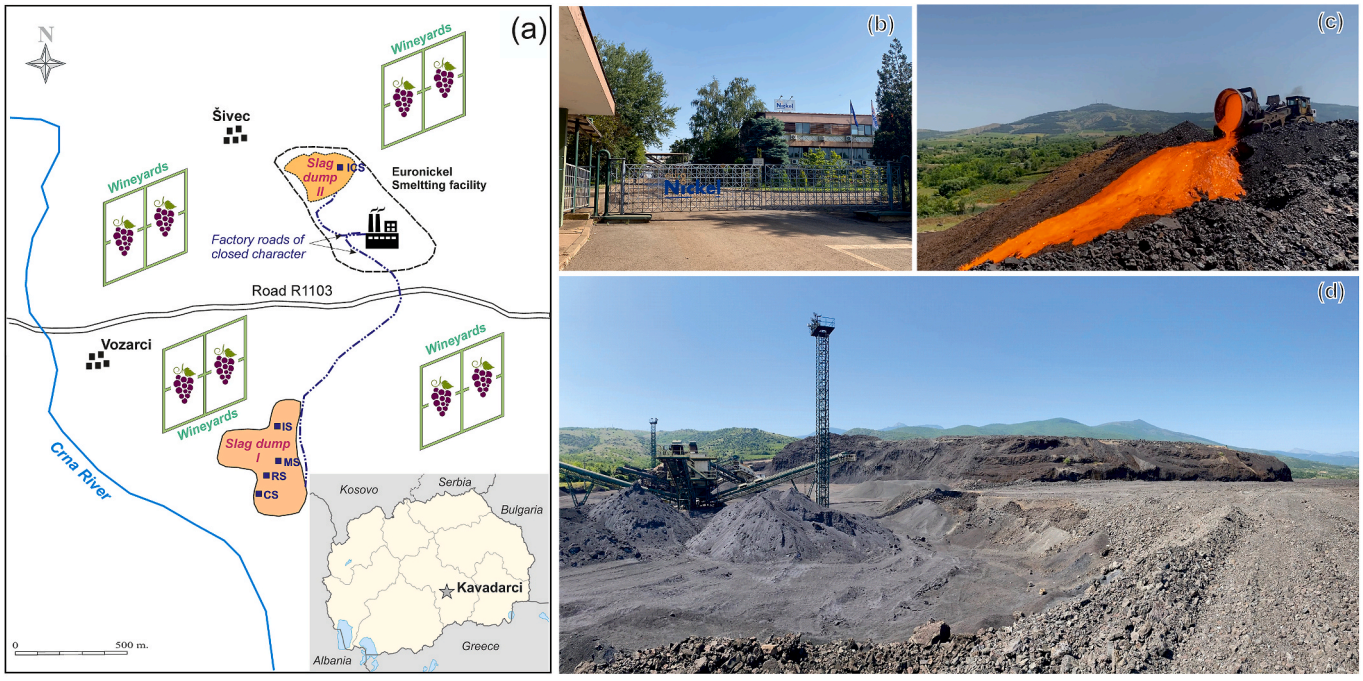

Fig. 1. (a) Location of the slag dumps including sampling points; (b) photographs of the main entrance to the Euronickel Industries GmbH; (c) slag dumping at the slag dump II near Šivec village, and (d) slag dump I near Vozarci village.

facility. The Ržanovo mine is a typical example of metamorphosed lateritic Fe-Ni ore redeposited in sedimentary basins (Serafimovski et al., 2013 and references therein), which was operated for almost 30 years, with several stoppages, and during that period produced 11.2 Mt of ore with an average grade of 0.92–0.94 % Ni.

The smelting installation is relatively new with advanced technological processes. Production was stopped for the first time in 1999, and then restarted in June 2001 under the company Feni Industry. Constant growth of metal production occurred in years to come, from 5100 metric tons (mt) in 2002 up to 20000 mt of nickel in the form of ferronickel in 2013.This capacity was kept up until today. In January 2018, the company Euronickel Industries completely acquired the smelting facility near Kavadarci.

All the equipment in the facility is designed to process 2 060 000 tons of nickel-bearing ore per year, which contains ~1.8% Ni and ~22% Fe and approximately 24% of moisture (Euronickel, 2021). The plant can produce 20 000 tons of nickel annually in the form of a ferronickel alloy, which contains nickel in amount of 20% up to 40% Ni (usually 20% Ni and 80 % Fe). Historically, the smelter used ore only from the Ržanovo Mine. Later however, it started using imported foreign ore from lateritic ore deposits in Indonesia, the Philippines, Guatemala, Turkey, Albania and from 2018, the production is mainly based on the lateritic ore from the Ivory Coast. Currently, a blend of Ivory Coast ore and Albanian ore is used, in ratio 75%–25%, respectively (Euronickel, 2021).

2.2. Slag sampling and sample preparation

The sampling of different solid slag dump materials was done in May 2022 as part of an Austria-North Macedonia bilateral scientific project. A maximum of 40 kg of material were collected. There are three different types of collected samples:

(a) *Electric furnace slags (EFS)* of various ages and from different source materials. Samples designated IS (N 41° 25,39′ E 021° 56,07′) (Figs. S1a and b) were imported between 2012 and 2017 from Indonesia, but also from the Philippines, Guatemala, Turkey, and Albania. The samples RS (N 41° 25′ 28.2″; E 21° 56′ 10.2″) were produced by smelting lateritic FeNi ore from the Ržanovo deposit (Serafimovski et al., 2013) (Figs. S1c and d), and they were exposed to weathering conditions for a maximum of 40 years. The samples designated ICS (N 41° 25′ 16.6″; E 21° 56′ 11.7″) (Fig. S1 e,g) are the slags from the current smelting process, which uses a mixture of the ore imported from Ivory Coast and Albania.
(b) *Converter slags,* of different ages denoted as CS (N 41° 24,24′ E 021° 56,11′) (Fig. S1 f,h)
(c) *Magnetic slags,* which came from the previous magnetic separation process when the smelting facility used ore from the nearby Ržanovo mine (Fig. S1 i). These samples are referred to as MS slags (N 41° 25′ 27.6″; E 21° 56′ 19.9″).

Different sample preparations were required for various analytical techniques. A portion of the samples that were chosen for the leaching experiments, bulk chemical and mineralogical analyses needed to be processed into homogenized rock powder, which was done by compounding rock powder pellets for powder X-ray diffraction (PXRD) and X-ray fluorescence (XRF) measurements. Using a jawbreaker, the slag material was first reduced in grain size to create the powder. This material was then ground using a swing mill until it was homogenized rock powder. To avoid contamination of the samples, a mill that was harder than the raw material had to be used. Here, an agate mill was employed. It takes about 10 min in the refiner to obtain a powdered material with a grain size of about 30–35 μm. This process was carried out following procedure of Nagl and Mader (2019): about 10 g of the homogenized rock powder were well-mixed for 10 min with 0.5 ml of aqueous polyvinyl alcohol by manual stirring. Afterward, they were pressed to pellets using a hydraulic press, reaching a pressure of 16 t/cm^2. Before measurement, the pressed pellets were dried in an oven at 70 °C overnight. Ten further samples were prepared as polished sections from the various hand specimens showing diverse external appearance, textures and display weathering crusts. They were used for Raman spectroscopy and SEM-EDX analyses. Their outward appearance played a role in their selection. After being cut, they were embedded in resin and polished with corundum.

2.3. Chemical analyses

2.3.1. X-ray fluorescence (XRF) analyses of the slags

The XRF analyses were performed on a sequential X-Ray spectrometer PHILIPS PW2404 with a super-sharp end-window tube with a Rh-anode and a programmable 4 kW generator (60 kV max., 125 mA max.; iso-Wattswitching), the accompanying software is PANalytical "SuperQ" vers. 5.1B (5.2822.3) with the options "Pro-Trace" and "Omnian" (Nagl and Mader 2019). These two different software modules, "Pro-Trace" and "Omnian" were used for this study, to analyze the data. Pro Trace works with specific standards and allows an accurate measurement of trace elements concentrations. Whereas Omnian provides a convenient and rapid quantitative analysis of major and minor elements without any standards. Omnian is based on a fundamental parameter calculation (Nagl and Mader, 2019). To overcome possible problems of drift during analysis, samples are run in groups and the count rates obtained are ratioed to monitor samples; a batch of quality control samples is also measured together with each group.

2.3.2. ICP-OES analysis of the leachates

The chemical composition of the leachates were determined with Inductively Coupled Plasma Optical Emission Spectrometer (ICP-OES, Avio 200, PerkinElmer). The following wavelengths were used for analysis of selected metallic elements: Zn 213.857 nm, Co 228.616 nm, Cu 327.393 nm, As 188.979 nm, Ni 231.604 nm, Cr 267.716 nm, V 311.07 nm, Mo 202.03 nm, Pb 220.353 nm, and W 207.912 nm. Calibration curves were prepared based on multi element standard solutions prepared from single element standard solutions (Merck). Conditions of analysis were as follows: plasma argon gas flow 12 L/min, auxiliary gas flow 0.2 L/min, nebulizer gas flow 0.7 L/min, power 1500 W, sample flow rate 1 ml/min. Diluted multielement standard solutions (Spex CertiPrep Multi Element Standards no 4 and no 2) were analyzed in order to check correctness of the calibration curves.

2.4. Mineralogical analyses

The samples selected for powder X-ray diffraction (PXRD) (the same samples on which XRF and leaching experiments were performed) were analyzed with a Bruker D8 Advance diffractometer (Cu-Kα radiation, Lynxeye detector, 40 kV, 25 mA, step scanning from 5° to 85° 2θ, room temperature, step size 0.01° 2θ, dwell time of 1 s per step). The DIFFRAC.EVA software, version 4.2, and the ICDD powder diffraction file PDF-2 were used for peak and phase identification. The secondary weathering products were scratched from the surface of the samples and have also been identified using PXRD.

Supergene phases (secondary weathering products) were separated under a binocular and identified by Raman spectra using a Horiba LabRam-HR system equipped with an Olympus BX41 optical microscope in the spectral range between 100 and 4000 cm^{-1} (632.8 nm He–Ne laser; 50 × or 100 × objective; N.A. = 0.90; exposure time between 5 and 60 s). Raman studies were performed both on the selected single-crystals or phase aggregates and on the on the polished sections.

Chemical composition and micromorphology of mineral phases were studied with a JEOL JSM-6610 LV scanning electron microscope (SEM) with tungsten filament (15 kV), equipped with an energy-dispersive X-ray (EDX) detector (Bruker e-FlashHR+, resolution 127 eV) and Bruker Esprit 2.0 software. Spectra were recorded for 60 s and with dead times

<5%. All SEM-EDS studies were performed on the carbon-coated polished sections of the hand specimens with intact weathering crusts. We also wanted to point out that the precision of the results of chemical analyses using SEM-EDX and electron microprobe analysis (EMPA) are not the same, but the accuracy of the standardless analyses (15 kV, 60 s measuring time, spatial resolution 0.1–1 μm, PB-ZAF correction) of the instrument we used is estimated to be 2–3% for "common" phases and better than 5–10% for "uncommon" phases with unusual chemical compositions. In the case of significant peak overlaps, where errors could exceed 10%, analytical results were compared to those of external standards.

2.5. Leaching experiments

The leaching experiments were carried out according to the toxicity characteristic leaching procedure 1311. The fraction size used for leaching experiment was 30–35 μm. Three replicates were implemented for the leaching experiments. Slag portions of 2 g were placed in polypropylene flasks and filled with 40 mL of extracting solutions 1 and solution 2. All the experiments run in parallel. Solution 1 was composed of 5.7 mL of acetic acid (CH_3CH_2OOH) and 64.3 mL of 1 M NaOH per 0.5 L of distilled water so that pH of solution was 4.93. Solution 2 was composed of 5.7 mL of acetic acid (CH_3CH_2OOH) per 1 L of distilled water so that pH of solution was 2.92. The extracting vessels were placed on a rotatory shaker and shaken for 18 h at ambient temperature. After termination of leaching experiments, the leachates were filtered using funnel filters in order to separate slag particles from leachate. Filtered leachate was acidified using HNO_3 and stored at 4 °C prior to ICP-OES analysis.

At this point, we should note that the slag particles disposed in the field are larger than the fraction used in the leaching experiments, implying that the actual slag reactivity varies from the simulated lab scale scenario. However, the use of small slag particles was intended to demonstrate its general leaching tendency as well as to compare the reactivity of different samples. As a result, our approach provides insight into model simulations for so-called worst-case scenarios that may occur during samples' exposure to weathering.

2.6. Statistical analysis

The concentration of elements leached from the slags under different pH conditions (2.9 vs. 4.9) were compared by means of the Student t-test or the Mann-Whitney test. Normal distribution of results was checked by means of the Shapiro-Wilk test and the homogeneity of variance was checked by means of the Levene test. Statistical analysis was performed in the Statistica 13 (StatSoft).

Table 1
Bulk chemistry of the selected slag samples measured using XRF.

Samples	IS A	IS B	IS C	RS	ICS	CS	MS
	Type 1					Type 2	Type 3
wt.% following absolute error in %							
SiO_2	43 ± 0.1	47 ± 0.1	47 ± 0.1	35 ± 0.1	42 ± 0.1	8.5 ± 0.08	5.6 ± 0.07
TiO_2	0.14 ± 0.01	0.1 ± 0.009	0.17 ± 0.01	0.1 ± 0.01	0.27 ± 0.02	0.039 ± 0.006	0.022 ± 0.004
Al_2O_3	5.8 ± 0.07	3.9 ± 0.06	5.8 ± 0.07	3.8 ± 0.06	5.5 ± 0.07	1.1 ± 0.03	0.61 ± 0.02
Fe_2O_3[a]	22 ± 0.1	21 ± 0.1	21 ± 0.1	40 ± 0.1	29 ± 0.1	76 ± 0.1	77 ± 0.1
MnO	0.72 ± 0.03	0.64 ± 0.02	0.73 ± 0.03	0.57 ± 0.02	0.61 ± 0.02	0.091 ± 0.009	0.059 ± 0.007
MgO	23 ± 0.1	23 ± 0.1	20 ± 0.1	13 ± 0.1	17 ± 0.1	3.7 ± 0.06	4.2 ± 0.06
CaO	3 ± 0.05	3.1 ± 0.05	3.2 ± 0.05	4.2 ± 0.06	3.5 ± 0.05	7.6 ± 0.08	8.4 ± 0.08
Na_2O	0.29 ± 0.02	0.14 ± 0.01	0.31 ± 0.02	0.44 ± 0.02	0.18 ± 0.01	0.17 ± 0.01	0.063 ± 0.008
K_2O	0.1 ± 0.01	0.11 ± 0.01	0.11 ± 0.01	0.16 ± 0.01	0.2 ± 0.01	0.12 ± 0.01	0.033 ± 0.005
P_2O_5	0.013 ± 0.003	0.012 ± 0.003	0.014 ± 0.004	0.02 ± 0.004	0.017 ± 0.004	0.23 ± 0.01	0.5 ± 0.02
SO_3	0.19 ± 0.01	0.16 ± 0.01	0.16 ± 0.01	0.23 ± 0.01	0.19 ± 0.01	2 ± 0.04	2.5 ± 0.05
Cl	0.021 ± 0.004	0.028 ± 0.005	0.035 ± 0.006	0.0069 ± 0.002	0.012 ± 0.003	0.01 ± 0.003	–
mg/kg							
As	8.8	1.5	2.2	12.8	3.3	5.0	2.6
Ba	72.3	73.7	84.9	58.3	176.3	14.7	13.3
Ce	<1	14.1	3.8	<1	14.5	8.0	4.1
Co	35.1	33.4	22.0	87.1	31.4	116.6	129.6
Cr	11831	9632	12548	17423	10247	4895	6691
Cu	17.0	14.3	13.8	33.1	16.4	72.2	86.0
Ga	<1	1.4	1.2	2.8	2.3	11.1	13.7
La	9.1	6.6	14.3	6.9	83.2	1.9	<1
Mo	2.6	<1	<1	<1	<1	17.6	171.4
Nb	1.1	0.6	1.2	1.6	3.5	0.8	0.7
Nd	8.1	17.2	8.3	16.9	44.9	8.0	6.4
Ni	735	395	174	66	503	1853	3019
Pb	8.2	18.7	8.1	5.0	9.9	3.4	2.1
Rb	4.4	4.8	4.7	7.5	9.2	4.4	<1
Sc	29.2	27.7	35.7	30.7	25.1	<1	<1
Sn	8.2	7.2	6.0	6.2	5.8	11.8	11.4
Sr	35.7	35.4	40.7	112	29.8	35.4	48.7
Ta	<1	<1	<1	<1	<1	<1	<1
Th	1.9	1.2	2.3	2.2	5.4	3.1	<1
U	1.4	0.0	<1	2.0	2.7	<1	<1
V	260	123	277	182	199	38.6	67.7
W	<1	<1	<1	<1	<1	19.0	21.8
Y	13.9	10.4	16.2	5.9	36.1	2.6	2.8
Zn	334	381	374	154	335	22.4	26.1
Zr	19.1	11.9	22.2	17.6	65.7	11.6	5.9

[a] Total Fe (FeO + Fe_2O_3) expressed as Fe_2O_3.

3. Results

3.1. Bulk chemistry

The chemical compositions of the slag samples are reported in Table 1. The EFS slags (samples RS, IS A–B and ICS) are mainly composed of SiO_2 (37–45 wt.%), Fe_2O_3 (21–40 wt.%), MgO (13–23 wt.%), followed my minor amounts of Al_2O_3 (3.8–5.8 wt.%) and CaO (3.0–4.2 wt.%). These slags are also significantly enriched in metals and metalloids: Cr (9633–17423 ppm), Ni (174–735 ppm), Zn (154–381 ppm) and V (123–277 ppm). As some of the metallic elements are present in various phases (silicates, glass, oxides, sulfides, metallic compounds), the sums of oxides are generally low and are not given in Table 1.

The converter slag (CS) and magnetic slag (MS) are exceedingly rich in Fe_2O_3 (76 and 77 wt.%), followed by smaller amounts of CaO (7.6 and 8.4 wt.%), SiO_2 (8.5 and 5.6 wt.%), MgO (3.7 and 4.2 wt.%) and SO_3 (2 and 2.5 wt.%). CS- and MS-slags are also enriched in Cr (4895 and 6691 ppm), Ni (1853–3019 ppm) and Co (117 and 130 ppm), respectively. Elevated concertation of Mo was also observed (CS: 18 ppm; MS: 171 ppm).

3.2. Bulk mineralogy

Although anthropogenic materials do not fulfill the criteria for minerals, we used mineral names for their synthetic equals, in order to provide a better picture of the solid phase composition. The overview of the identified slag phases is given in Table 2.

The phases identified within the slags can be divided into following groups: (i) primary slag phases that formed during slag crystallization (silicate, oxide, glass); (ii) relict ore, gangue and flux minerals from the original smelting charges (ie. sulfides, intermetallic compounds), and (iii) secondary slag minerals that crystallized during weathering of the slag. Nevertheless, the slags largely consist of primary phases.

PXRD studies (supplementary material, Figs. S1–S3) showed substantial differences in the phase composition between different categories of the EFS. RS-samples, which at the same time represents the oldest slags (~40 years old), are predominately composed of olivine-type phases (mostly Fe-rich forsterites), followed by significant amount of the spinel-group minerals (chromite, trevorite, nichromite) and minor clynopyroxene-group phases (augite, diopside) (Fig. S2). EFS gained from smelting of the predominantly ores imported from Indonesia (IS A-C) (Fig. S3) are composed mostly of olivine-group phases (Fe-rich forsterites and minor Mg-rich fayalites), pyroxene-group phases (enstatite, pigeonite) and residual glass. Besides olivine-group compounds, the newly formed slags (ICS-samples) are rich in glass-phase, followed by the minor pyroxene-group minerals (enstatite) (Fig. S3). Convector slag (CS) is composed of hematite, magnesioferrite, Ca-sulphates (gypsum and anhydrite) and minor silicates (pigeonite, kirschsteinite) and calcite (Fig. S4). MS-slags are mostly composed of magnesioferrite, wüstite and hematite, followed by minor Ca-silicates (Fig. S4).

3.3. Crystal chemistry of the individual slag phases

Further mineralogical investigations of the polished section, using a combination of SEM-EDX analyses and micro-Raman spectroscopy, enabled us to describe the crystal chemistry of the slags' major and minor components.

3.3.1. Silicates

The EFS is primarily composed of crystalline silicate phases. In all EFS-samples, the dominant silicate phases are olivine-group compounds (Fig. 2a and b), represented by the solid-solution between forsterite (Mg_2SiO_4) and fayalite (Fe_2SiO_4) with minor substitutions of Cr: 0.1–0.4 at.%, Mn: 0.1–0.3 at.% and Ca: 0.1–0.3 at.%. However, the majority of the olivine-type phases were characterized as Fe-bearing forsterite, with Fe-content ranging between 3.1 and 13.3 at.% (Table S1). The second dominant silicate phases are pyroxene-group minerals (Fig. 2c and d), represented by the solid solution between enstatite ($Mg_2Si_2O_6$) and ferrosilite ($Fe_2Si_2O_6$) with minor substitutions of Ca (up to 2.5 at.%), Al (up to 2.5 at.%), Cr (up to 0.7 at.%) and Mn (up to 0.3 at.%). The majority of pyroxene phases were characterized as Fe-bearing enstatite (Fe: 2.1–6.5 at.%), where just a few could be identified as Mg-rich ferrosilite

Table 2
The overview of the slag phases characterized with PXRD, SEM-EDX and Raman spectroscopic analyses.

Sample	Color of the powdered samples	Silicates/glasses	Oxides	Sulfides and intermetallic phases/alloys	Weathering products and other phases
IS A	Light greenish-grey	Forsterite (Fe)[a–c] Ferrosilite (Mg)[1a,b]; Enstatite[a–c]; Pigeonite[1]; amorphous glass	Magnesiochromite[b]; Fe-oxide[b], wüstite[b]	Pyrrhotite[b]; Petlandite ($Ni_5Fe_3S_7$)[b]; Ni_6Fe_4/FeNi/Fe_7Ni_3/Fe[b]	Ni-bearing hydroxy-iron-oxides (HFO)[b]
IS B	Very light grey	Forsterite (Fe)[a–c] Clinoenstatite[a–c]; Pigeonite[a] Augite-diopside[a], amorphous glass	Magnesiochromite[b]; Fe-oxide[b], wüstite[b]	Pyrrhotite[b]; Petlandite ($Ni_5Fe_3S_7$)[b]; Ni_6Fe_4/FeNi/Fe_7Ni_3/Fe[b]	Ni-bearing hydroxy-iron-oxides (HFO)[b]
IS C	Light grey	Forsterite (Fe)[a–c]; Enstatite[a–c]; Pigeonite[a]; Cristobalite[a], amorphous glass	Magnesiochromite[b]; Fe-oxide[b], wüstite[b]	Pyrrhotite[b]; Petlandite ($Ni_5Fe_3S_7$)[b]; Ni_6Fe_4/FeNi/Fe_7Ni_3/Fe[b]	Ni-bearing hydroxy-iron-oxides (HFO)[b]
RS	Middle grey	Forsterite[a–c], Diopside[a], amorphous glass	Magnesiochromite[a–c]	Fe_9Ni[b]	Calcite[c]
ICS	Light grey	Forsterite[a–c]; Enstatite[a–c], amorphous glass	Magnesiochromite[b,c], Magnetite[b]	Pyrrhotite[b]; Fe_7Ni_3 to Fe_9Ni/$Fe_{9.5}Ni_{0.5}$ with Co-traces[b,c]; $Cu_{44}S_{42}Fe_{14}$[b]; Chalcopyrite ($CuFeS_2$)[b]	HFOs and Ni-bearing HFOs[b]
CS	Reddish-brown	Kirschsteinite[a], Pigeonite[a], Calcio-olivine/Larnite[b]	Magnesioferrite[a–c], Hematite[a–c]	Pyrrhotite[b]	Gypsum[a–c], Anhydrite[a,c], Sulfur[a], Syngenite[a,c], Aphthitalitea,c, Powelite[b], $Ca_3(PO_4)_2$–$2Ca_2SiO_4$[b,c]
MS	Dark grey to black	Larnite[a]	Magnesioferrite[a–c], Hematite[a–c]; Wuestite[a,b]; Magnetite[b]; Trevorite[b]; Magnesiochromite[b]	Pyrrhotite[b]; Fe_7Ni_3[b]; Petlandite ($Ni_5Fe_3S_7$)[b];	HFOs and Ni-bearing HFOs[b]

[a] PXRD.
[b] SEM-EDX.
[c] Raman.

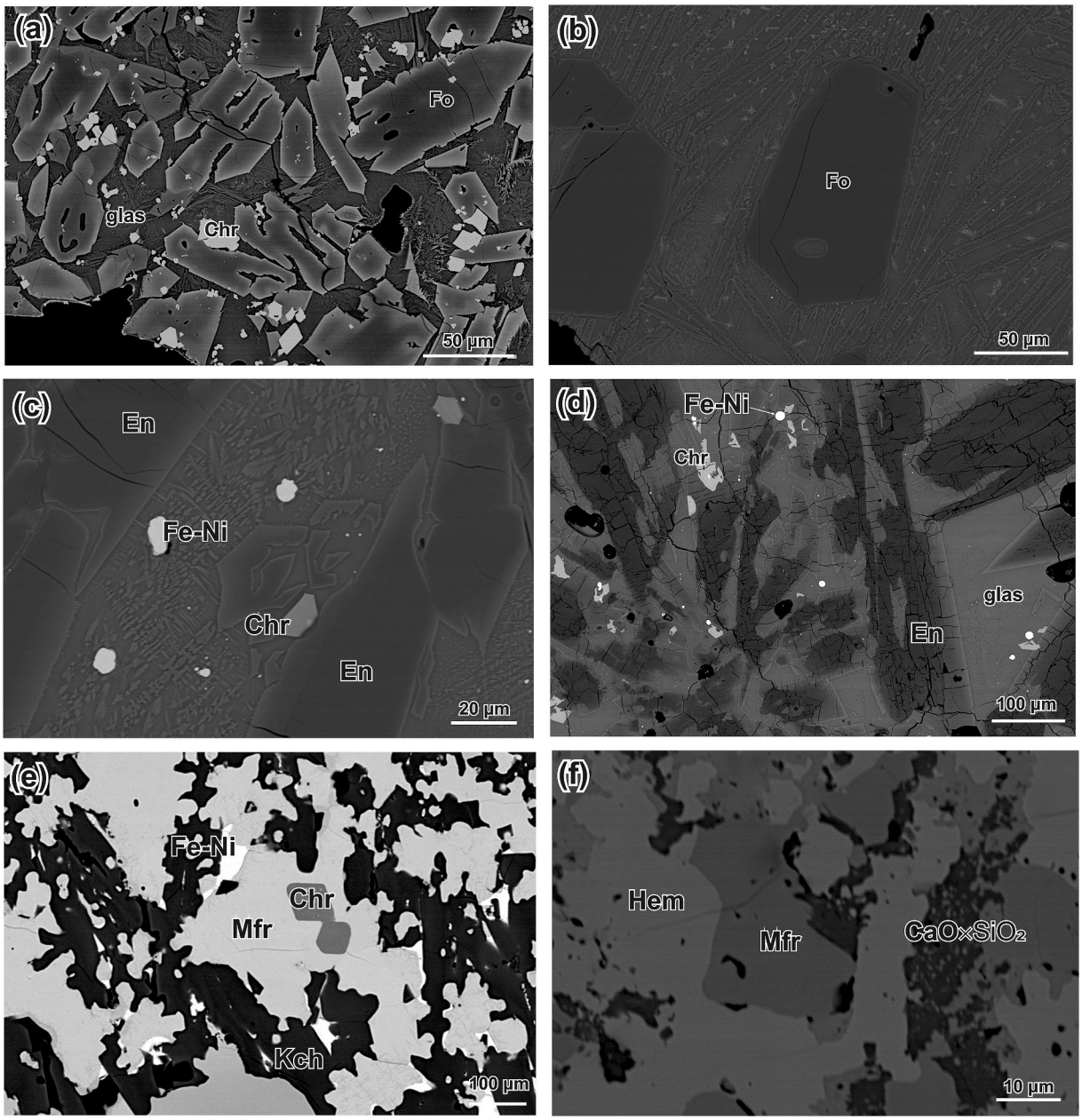

Fig. 2. Scanning electron microphotographs (in backscattered electrons-BSE) of the polished sections with emphasis on silicate and oxide phases. (a) euhedral forsterite (Fo) and chromite (Chr) single-crystals (RS-sample) imbedded in the glass-matrix; (b) Euhedral forsterite crystals and forsterite laths in the glass-matrix (sample IS); (c) euhedral enstatite (En) in the glass, where $Fe_{94}Ni_5Co$ round aggregates and chromite are trapped; (d) big enstatite laths in glass, where Fe-Ni droplets and chromite crystals are imbedded (ICS sample); (e) magnesioferrite (Mfr) intergrown with kirschteinite (Kch) and Fe_7Ni_3 aggregates in MS-sample. Euhedral chromite crystals are trapped in magnesioferrite; (f) intergrowth of magnesioferrite (Mfr), hematite (Hem) and larnite ($CaO{\cdot}SiO_2$).

(Mg: 8.8–11.6 at. %). These two silicate phases are absent in the CS and MS-samples. In the RS samples, Fe-rich forsterite form both large crystals (up to 400 μm in length), as well as smaller dendritic crystals. These are embedded in the glass matrix (Fig. 2a). Microscopic investigations did not show any presence of enstatite-ferrosilite series in the RS-samples (Table S1) but PXRD studies confirmed presence of enstatite. In the IS (A-C) samples, Fe-bearing forsterite is again the dominate silicate. It appears in the form of large crystals and laths embedded in the glass matrix (Fig. 2b). Enstatite crystals were observed as large crystals embedded in the glass matrix together with dendritic olivine (Fig. 2c). In the ICS-samples, the dominant silicate phases are Fe-bearing enstatite and forsterite embedded in the glass matrix. They usually appear in the form of large crystals (up to 300 μm in length), but also as smaller dendrites embedded in the glass matrix (Fig. 2d). In the MS-samples, the main phases are oxides and they are embedded in the polycrystalline silicate matrix mostly built from Mg-rich kirschsteinite, $CaFe^{2+}SiO_4$ with Mg-content ranging between 4.6 and 5.1 at.% (Fig. 2e). In the CS samples, the main phases are magnesioferrite, $MgFe_2^{3+}O_4$ and hematite, Fe_2O_3, embedded in the Ca-silicates (chemically $CaO{\cdot}SiO_2$) (Fig. 2f). These silicates are either representatives of calico olivine or larnite, Ca_2SiO_4, some of the bearing the significant amounts of sulfur (4.3 at. %).

3.3.2. *Silicate glass*

The presence of silicate glasses was found primarily in the EFS samples. The chemical composition of the glass phase varies but is consistent across all slag samples studied (Table S2). The main components are Si (20.2–23.3 at.%), Al (4.1–9.1 at.%), Fe (3.2–8.9 at.%), Ca

(2.7–6.2 at.%), and Mg (0.9–4.8 at.%). Local enrichment in Mo (up to 0.2 at%) and Cr (up to 0.4 at%) was observed in the ICS samples. It was not possible to demonstrate the presence of Ni or Co in glasses. PXRD analyses show that ICS samples are the richest in glass.

3.3.3. Oxides

Oxides were identified in all types of slags and are primarily present as spinel-type compounds (chromite and magnesiochromite, as well as minor magnetite, and trevorite). They are, however, major constituents of CS and MS slags. Chemical composition of the oxide-phases is given in Table S3. Spinel-group phases in the EFS-samples are represented with Mg-bearing (5.5–9.7% at.%) chromite showing significant presence of Al (3.3–12.2% at.%), (Fe,Mg) $(Cr,Al)_2O_4$ (Table S3). They form both dendritic and euhedral crystals up to 30 μm and are usually embedded in the glass matrix and in the olivine-type crystals (Fig. 2a–c,d). Chromite from RS-sample with Al up to 3.9 at.% form only euhedral crystals up to 50 μm in length and embedded in olivine and glass (Fig. 2a). Magnetite and Ni-bearing hydrous ferric oxides (HFO) (Ni: 1.1–8.3% at.%; Si: 0–2.6 at.%), as well as crystalline iron(oxy)hydroxides, including hematite, were also found in the IS-samples. The dominant phases in the CS samples are magnesioferrite, and hematite (Fig. 2f). They are one of the three main phases of CS slags, along with Ca-silicates. Magnesioferrite can have up to 4.3 at.% Ni and 1.1 at.% Cr, while magnetite can have up to 1.3 at.% Co and 1.3 at.% Cr. The primary phases in MS samples are Ni-bearing magnetite (Ni: 1.6–12.1%), magnesioferrite, and wüstite, FeO with minor Mg-bearing chromite (Mg up to 6.1%). These three phases are embedded in the Ca-silicate matrix, where they are intergrown and sporadically exhibit weathering products (Ni-bearing HFOs) along cracks and rims (Fig. 2).

3.3.4. Sulfides and intermetallic compounds

The silicate matrix contains numerous droplets of metallic and sulfide phases: (1) larger inclusions (<100 μm in size) (Fig. 3a and b) and (2) small droplets (often less than several μm in size) (Fig. 2a–c,d and Fig. 3c and d), embedded in the glass and olivine phases. The large inclusions are commonly composed of sulfides intergrown with intermetallic alloys (Fig. 3a and b).

The most common and the most abundant sulfides are pyrrhotite, $Fe_{1-x}S$, pentlandite, $(Fe,Ni)_9S_8$ and Fe-bearing heazlewoodite, Ni_3S_2 (Table S4). Pyrrhotite contains significant amounts of Ni and Co (IS up to 1.9 at.% Ni and 1.4 at.%; ICS up to 3.3 at.% Ni and 1.2 at.%; CS up to 2.4 at.% Ni an 1.3 at.% Co). Furthermore, trace amounts of Cu-Fe-sulfides have been observed in the ICS-samples (Fig. 3b; Table 4S). Their chemical composition based on the SEM-EDX measurements best correspond to bornite, Cu_5FeS_4 and chalcopyrite, $CuFeS_2$ (Table S4).

Intermetallic compounds belong to the binary Fe–Ni system, where Fe:Ni ratio varies from 1:0 to 2:3 (Table S5). Ni-rich members correspond to awaruite, Ni_3Fe are present only in IS slags. They contain significant amounts of Co (0.7–2.9 at.%) and minor amounts of As (0.7 at.%). Sulfides and intermetallic phases have been identified using the combination of SEM-EDX analyses and Raman spectroscopy (Table S4; Fig. S4).

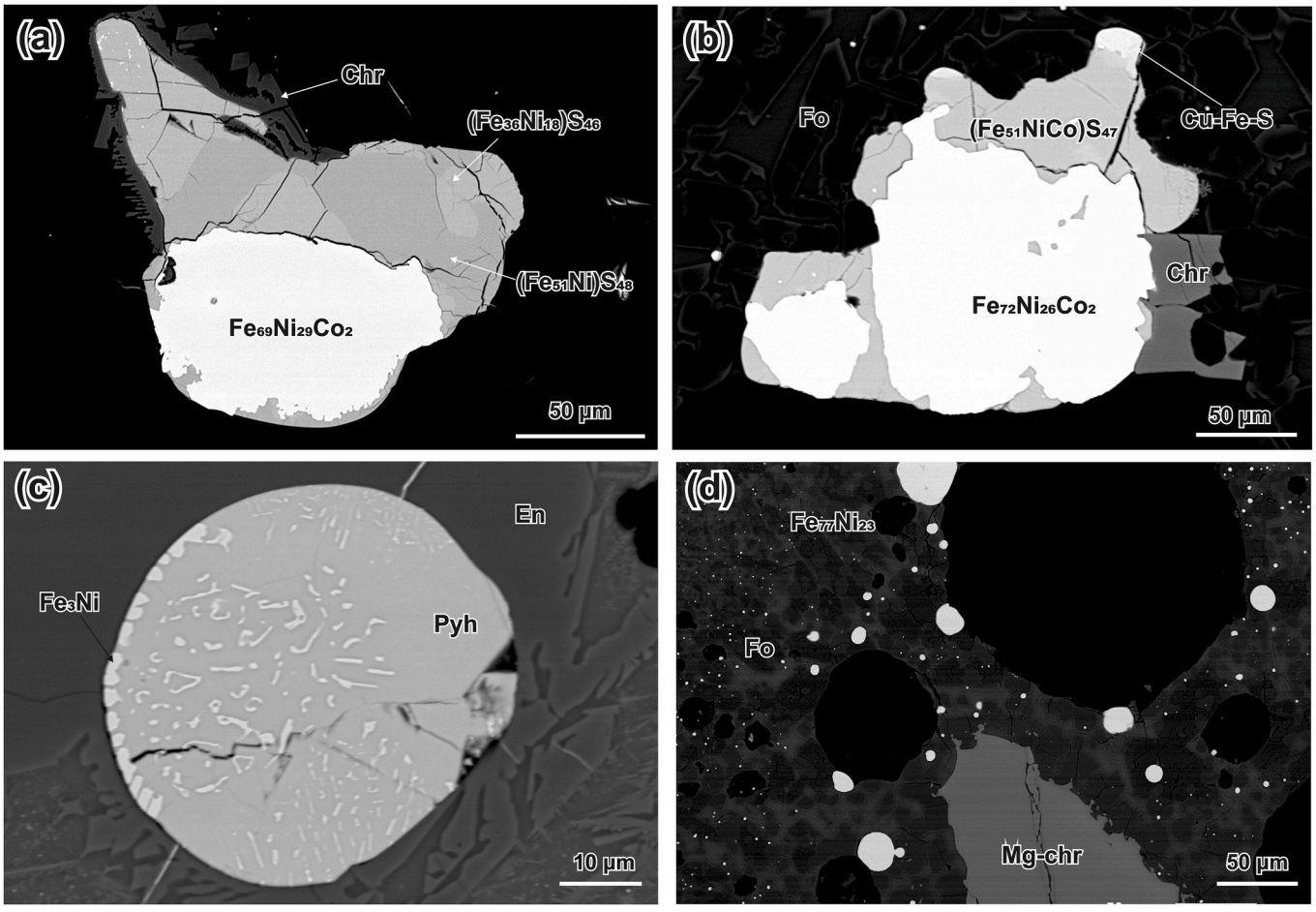

Fig. 3. BSE-images of the polished sections showing predominately sulfide and intermetallic phases. (a) Intermetallic compound $Fe_{69}Ni_{29}Co_2$ intergrown with Ni-bearing pyrrhotite in glass matrix of ICS slag; (b); (c) Intermetallic compound Fe_3Ni trapped in pyrrhotite (Pyh) embedded in enstatite crystal of IS slag; (d) overview micrograph showing smaller and bigger droplets of the intermetallic compound $Fe_{77}Ni_{23}$ embedded in the enstatite-glass matrix, where magnesiochromite (Mg-chr) is also trapped.

3.3.5. Weathering phases and mineral efflorescence

The slags have been subject to weathering and oxidation since their dumping, some of them since the late 1980s. Weathering phases, especially from the EFS are dominated by iron oxides, iron hydroxides and HFO (Fig. 4a–d). Most of them, especially HFOs are Ni-bearing, where Ni reach values between 1.0 and 8.3 at.% (Table S3).

CS and RS slags show a series of mineral efflorescences. They most commonly occur as powdery or cemented salt precipitates at seepage points at the base of the dump (Fig. S1 f), but also as the crust-like surface coatings and solid pore fillings of slag fragments. Mineral efflorescence on the crest and top surface of the dump are rare and occur on glassy slag surfaces, fillings within slag pores, coatings in fractures and on exposed sulfide ore aggregates embedded in the slag.

Mineral efflorescences from the seepage points of the CS and RS samples are of light greenish to yellow, yellow and white colors (Fig. S1 f,h). These crusts were scratched from the surface of the samples and have been analyzed with both PXRD (Fig. 5) and micro-Raman spectroscopy (Fig. 6). White-yellow solid crusts on the surface of the CS-slags (Fig. S1 f,h) consists mostly of the sulfate phases: gypsum, $CaSO_4 \bullet 2H_2O$, anhydrite, $CaSO_4$ syngenite, $K_2Ca(SO_4)_2 \bullet H_2O$ native sulfur, S, and aphthitalite, $(K,Na)_3Na(SO_4)_2$. (Figs. 5 and 6). The white crusts on the surface of the RS samples do not contain other major minerals than calcite, $CaCO_3$.

3.3.6. Other phases

Besides the above-mentioned phases in the CS sample, we have

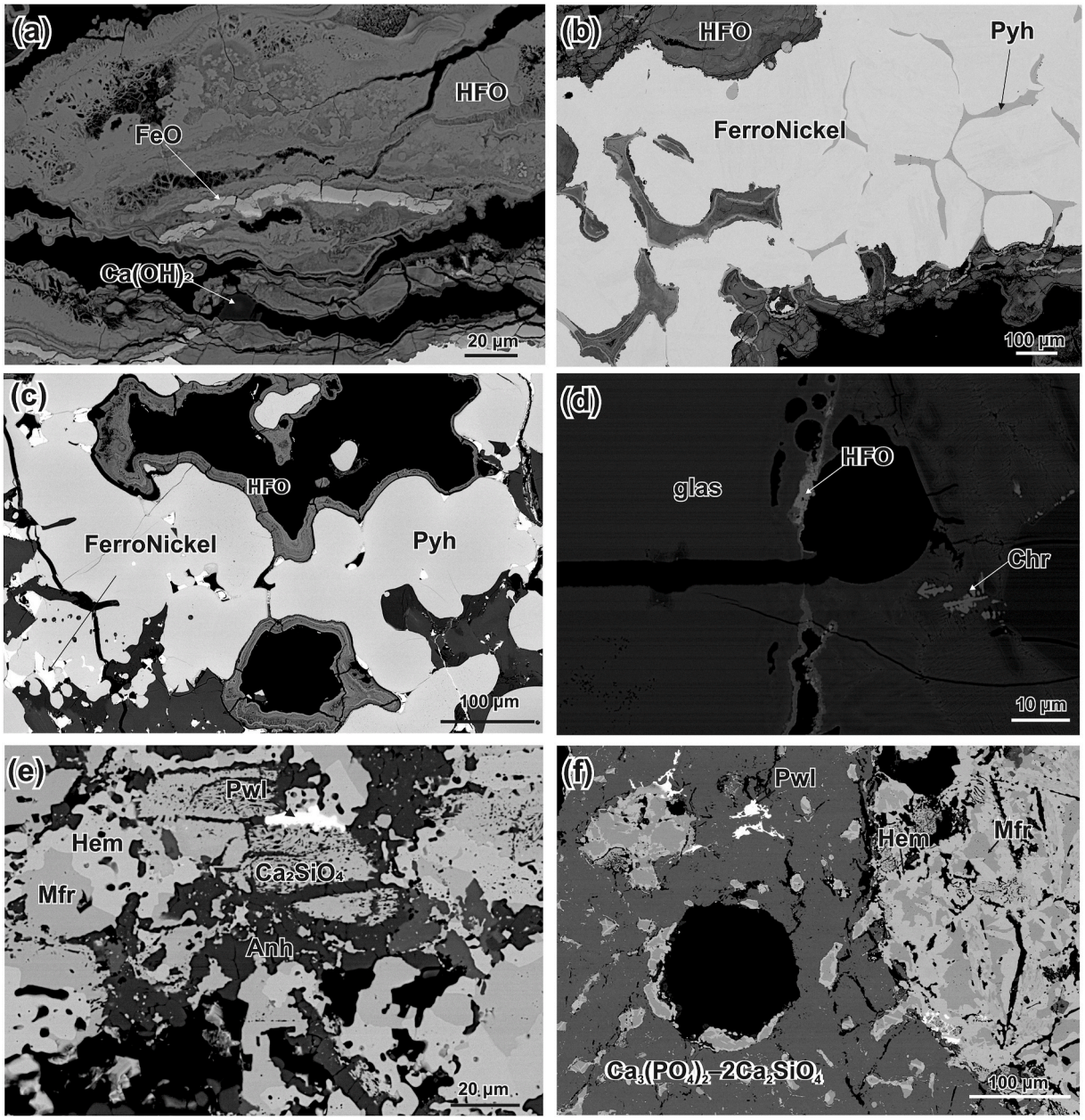

Fig. 4. BSE-images of the polished sections showing Early-stage weathering phases and other phases. (a) hydroxyl iron oxides (HFO) of various compositions (grey) and the relicts of wüstite (FeO) (light grey) and $Ca(OH)_2$ dark grey in the IC slag; (b) metallic iron-nickel intermetallic compound (bright white) overgrown with pyrrhotite (Pyh) (light grey) weathers to secondary HFO (dark grey) in the IC slag; (c) pyrrhotite (light grey) with droplets of intermetals Fe-Ni compound weathers on the rim to HFOs in the MS slag; (d) glass (dark grey) weathering observed in external parts of a ISC-slag fragment with weathering phase being HFO (light grey); (e) small powelite (Pow) aggregate intergrown with Ca-olivine, magnesioferrite (Mfr), hematite (hem) and anhydrite (Anh) aggregates in the CS sample; (f) Powelite aggregates in the $Ca_5(PO_4)_3$–$2Ca_2SiO_4$ phase of the CS sample.

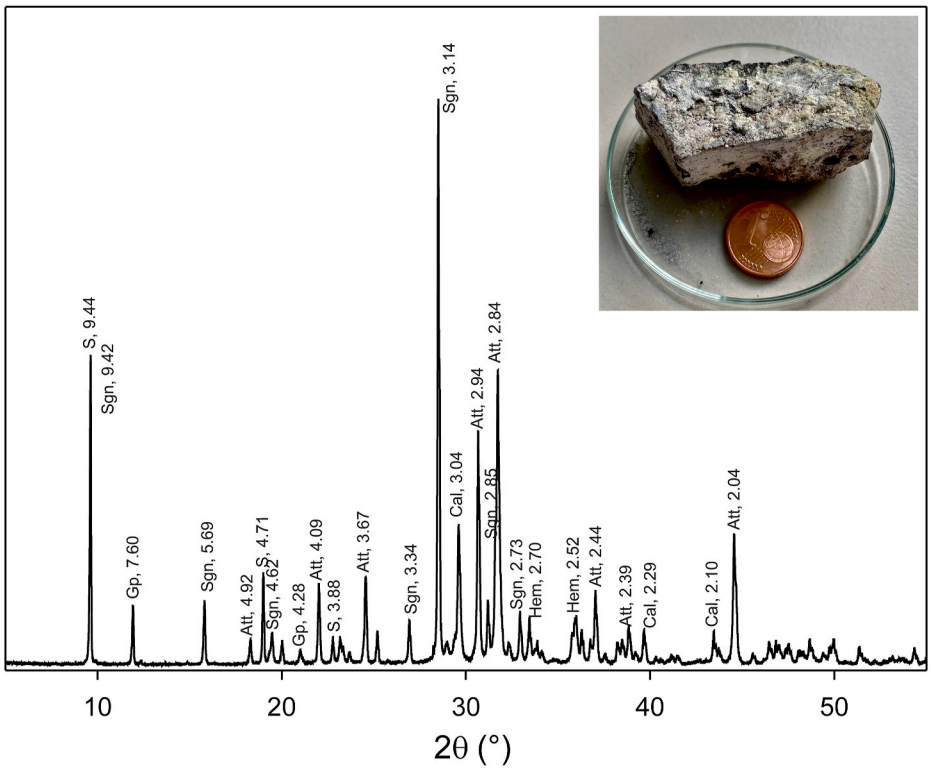

Fig. 5. Powder X-ray diffractogram of the phases scratched from the surface of the CS slag and macroscopic CS slag sample with visible evaporative mineral precipitates. d-values (Å) are given next to the phase abbreviations. Abbreviations: Att – aphthitalite; Cal – calcite; Gp - gypsum; Hem – hematite, S – sulfur, and Sgn – syngenite.

identified, anhydrite, as one of the major constituents of the CS slag (Fig. 4e), powelite, $CaMoO_4$ and calcium phosphate silicate (CPS) (Fig. 4f). According to SEM-EDX analyses (Table S6), powellite incorporates between 1 and 2.5 at.% Fe, 0.4–1.6 at.% W, and up to 0.2 at.% of Sr. CPS is ceramic-like compound belonging to the $Ca_3(PO_4)_2$–$2Ca_2SiO_4$ system and incorporates up to 2.8 at.% S, and up to 1.1 at.% Fe. Two EDX-analyses of the CPS showed the presence of F (2.8 and 3.0 at.%). Raman spectrum of CPS (Fig. 6) depicts presence of both PO_4 stretching vibrations (951 cm^{-1}) as well as SiO_4 (846 cm^{-1}) stretching vibrations.

3.4. Leaching behavior

Results of the leaching carried out according to the toxicity characteristic leaching procedure demonstrated higher leaching of metallic elements under acidic conditions (pH 2.9) than under slightly acidic conditions (pH 4.9) with some exceptions i.e. V for CS (Supplementary materials Fig. S6). The leaching of elements is displayed in Fig. 7. Slag immersion in the acidic solution (pH 2.9) resulted in metal leachabilities at up to 590 mgNi/kg from sample IS A, 2.2 mgAs/kg from sample MS, 44.9mgCr/kg from sample IS B, <0.1 mgPb/kg from all samples studied. These slags exposed to pH 4.9 released up to 530 mgNi/kg (IS A), 1.7 mgAs/kg (MS), 7.4mgCr/kg (IS B). Among the other elements up to 36.7 mgCo/kg (IS A), 21.2 mgMo/kg (MS), 12.9 mgZn/kg (IS A) under pH 2.9 and up to 29.0 mgCo/kg (IS A), 11.0 mgMo/kg (MS), 7.4 mgZn/kg (IS A) under pH 4.9.

4. Discussion

4.1. Origins of the slag variety and phase formation in slags

Differences in the chemical compositions between the various electric furnace slags (EFS) reflect both variations in the starting mixtures of ores, but certainly also the variation in furnace charges and smelting conditions over time. For instance, the RS sample, contrary to the other EFS samples, is significantly enriched in Fe (40 wt.%) and is depleted in Mg (13 wt.%) and Si (35 wt.%). This slag also shows the highest Cr (17 423 ppm) content. In addition to the dominance of spinel of the chromite type, microscopic examination revealed the massive presence of Fe-rich forsterite (Table S1), which appeared as large, well-developed crystals (up to 300 μm in size) as well as dendritic aggregates in the glass matrix. The large forsterite crystals crystallized mostly from silica of the melt, preventing significant residual glass formation at higher concentrations. Through the formation of spinel-type compounds (crystallizing after olivines), the slag melt solidified even more (mostly Mg-rich chromite). SEM-based analyses (Table S1) show that clinopyroxene phases are entirely absent in the RS-slag, and PXRD analyses (Fig. S1) verified only the presence of diopside. This, along with the degree of slag crystallinity, indicates that the slag melt, when smelter used the Rzanovo ore (RS samples) cooled slowly. Bulk chemical composition of the RS samples is very similar to results given by Boev and Bermanec (2005) for the slags mainly originating from processing of the ore from Ržanovo mine. Chemical composition for IC (A-B) and ICS samples are in accord with some former studies of the Euronickel (former Feni Industry) slags in regards to Fe_{tot}, SiO_2, MgO, Al_2O_3, CaO and Ni (Spirovska, 2010) and slight difference (10–15%) in comparison to results given in Ljatifi et al. (2014). The mineralogy of the IS and especially ICS samples, where we observed pronounced formation of the glass phase, indicates high smelting temperatures (1500–1600 °C) and rapid cooling of the melt by water quenching (Warner et al., 2006; Crundwell et al., 2011).

The bulk chemical compositions of the Euronickel slag contain much lower amounts of PTEs when compared to base-metal smelting slags, such as nonferrous slag from base-metal sulfide ores (e.g., Cu, Ni, Pb, and Zn) (Piatak et al., 2015, 2021 and references therein). In contrast, the concentrations of the PTEs of interest (Ni, Co, and Cr) match those of other slags from the processing of both sulfide and laterite Ni ore,

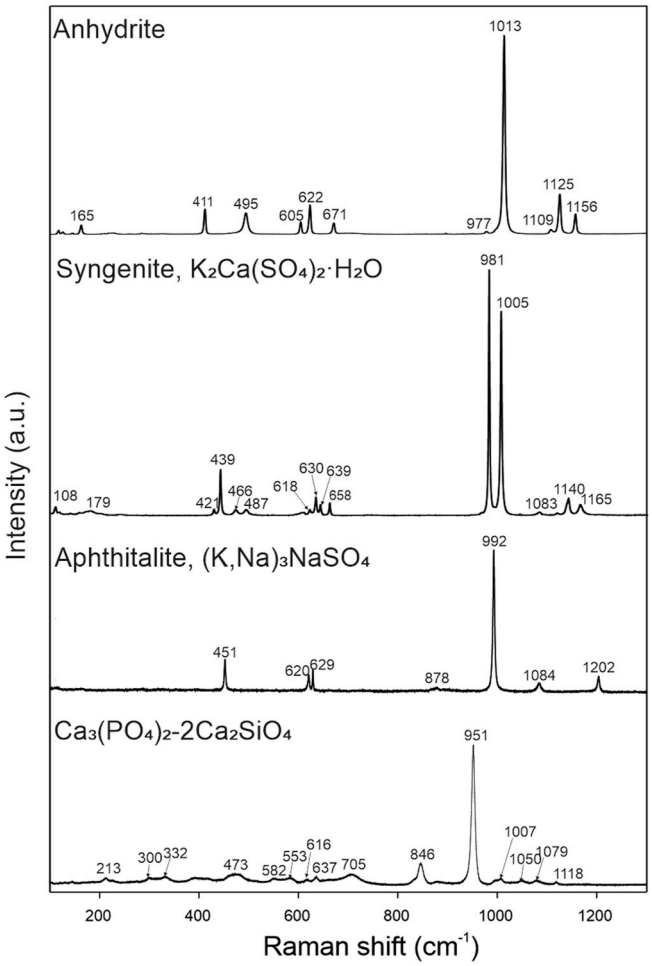

Fig. 6. Raman spectra of the mineral efflorescence on the seepage point of the CS samples and Raman spectrum of the $Ca_5(PO_4)_3$–$2Ca_2SiO_4$ (CS slag).

containing, respectively, 174–3019 mg/kg Ni, 22–130 mg/kg Co, and 4895–17,423 mg/kg Cr (Kierczak et al., 2009; Li et al., 2009; Perederiy et al., 2011; Ettler et al., 2016). In terms of silicate phases Euronickel slags are less complex than those from laterite Ni ores in Poland (Kierczak et al., 2009), but are very similar to the slags from the smelting of lateritic ores from Niquelândia in Brazil (Ettler et al., 2016). Euronickel slags contain up to 0.4 at.% Cr in glass phase, but no Ni, as observed in the studies by Lastra et al. (1998) and Kierczak et al. (2009). While Kierczak et al. (2009) demonstrated that pyroxenes are Ca-rich (hedenbergite, diopside, and augite) with up to 2.3 wt.% of Cr_2O_3, pyroxenes from the Euronickel slags are Mg-dominant (enstatite) with up to 0.7 at.% of Cr. Euronickel silicates do not contain any Ni. Besides sulfides and intermetallic compounds, Ni is concentrated in oxides (up to 8.3% Ni in HFO and up to 4.3 at.% Ni in magnesioferrite). The metallic phases present in our slag are of various chemical composition reaching from Fe, over Fe_7Ni_3 to Ni_3Fe composition, and the form through quenching at the temperatures <1440 °C (Swartzendruber et al., 1991).

Here we want to point out that nickel concentrations in the EFS slag samples (IS A-C, ICS and RS) (174–735 ppm Ni) may suggest an equivalent of approximately 93% nickel recovery in the smelting process (Warner et al., 2006; Crundwell et al., 2011; Perederiy et al., 2011). This fact was recently confirmed as production reality by the Euronickel's management team in informal discussion in September 2023.

4.2. Slag weathering

Some of the Euronickel slags have been weathering naturally for at least 40 years. Weathering phases are dominated by iron oxides, iron hydroxides, iron oxy-hydroxides (HFO), minor Ca-hydroxides, carbonates (calcite), and calcium sulfates (gypsum and anhydrite).

Weathering has no effect on the spinel-type phases, which are primary carriers of Cr. As a result, Cr in these phases can be considered immobile. The presence of unweathered olivine and chromite crystals suggests that silicates and oxides were more resistant to weathering than glass. Similar observations were noted for slags exposed to weathering conditions for at least 30 years in Szklary (Southwestern Poland) where slags are by-products of lateritic Ni-ores smelting (Kierczak et al., 2009).

Although sulfides and alloys are minor components in Euronickel slags, they are highly reactive and high in PTE, which may be released during weathering. Because intermetallic compounds occur mostly within sulfide grains, they may be subjected to weathering after degradation of the sulfides. Weathering and oxidation of sulfide-bearing slags results in the formation of sulfates, mostly present as mineral efflorescence on the surface of the converter slags. HFOs and Ni-bearing HFOs (Table S2; Fig. 4) are typical weathering products in the EFS-slags. They are both visible on the surface of the RS and MS-slags (oldest slags from the smelting of local Ržanovo ore), but are also present in all other slag types. This is because numerous Fe-bearing silicates (olivine, pyroxene) and oxides (spinel) as well as Fe-rich sulfides (pyrrhotite) occur commonly in these slags. Secondary HFO form because of the oxidation of Fe^{2+} to Fe^{3+} with subsequent hydrolysis of Fe^{3+} and precipitation of HFO.

On the surface of the CS slags, a more diverse spectrum of secondary phases is observed, including a variety of sulfates (Figs. 6 and 7). Sulfate phases (gypsum, anhydrite, syngenite, aphthitalite) form because the system is saturated with sulfate ions that formed after sulfides are oxidized. Formation of secondary HFO and sulfates may influence the further weathering of slags because the former generates acid and the latter consumes acid. However, the acid consumption caused by the sulfate precipitation is rather temporary because these phases are often soluble and their redissolution will release the acidity. In contrast to acid generation from the formation of HFO and dissolution of sulfates, the precipitation of calcite from the weathering of Ca silicates consume acid, leading to the alkaline conditions associated with these slags, which was confirmed by the near-neutral and slightly alkaline pH of both CS and MS samples.

4.3. Environmental implications

Fig. 7 shows the leached amounts of the contaminants (Pb, As, and Cr) and compares them to the regulatory levels. Other elements (Zn, Co, Cu, V, and Mo) have also been studied. Even though the norm does not anticipate the interpretation of these elements, we saw it as a general insight into the susceptibility of slag to leaching. We discovered that the analyzed contaminants did not exceed the regulatory limits set by the US EPA [US EPA, Office of Solid Waste (OSW), Catalog of Hazardous and Solid Waste, http://www.epa.gov/epaoswer/osw]. Most samples showed greater leaching in treatments with lower pH conditions (2.9) rather than at pH 4.9. The most noticeable difference between these treatments was observed for Ni, where leaching at low pH 2.9 was up to 135 times higher (MS) than at pH 4.9. Other contaminants leached up to 4–76 times faster at lower pH than at 4.9 pH. The Cr was mostly associated with magnesiochromite, indicating that this phase is major phase prone to solubility in a long term under weathering factors. In general, chromite is resistant to weathering. However, studies of chromites in ultramafic complexes evidenced that chromite can undergo chemical weathering leading to liberation of Cr^{3+} (Garnier et al., 2008). Furthermore, chromites can be occluded as nanoparticles in silicates. Silicates are more prone to weathering relative to chromites leading to release of nanoparticles of chromites (Bolaños-Benítez et al., 2018). Afterward, chromites can undergo weathering, and Cr^{3+} can be leached to solutions migrating in slag heap. Chemical reactions involving Cr are environmentally important since Cr^{6+} is considered as a very toxic form

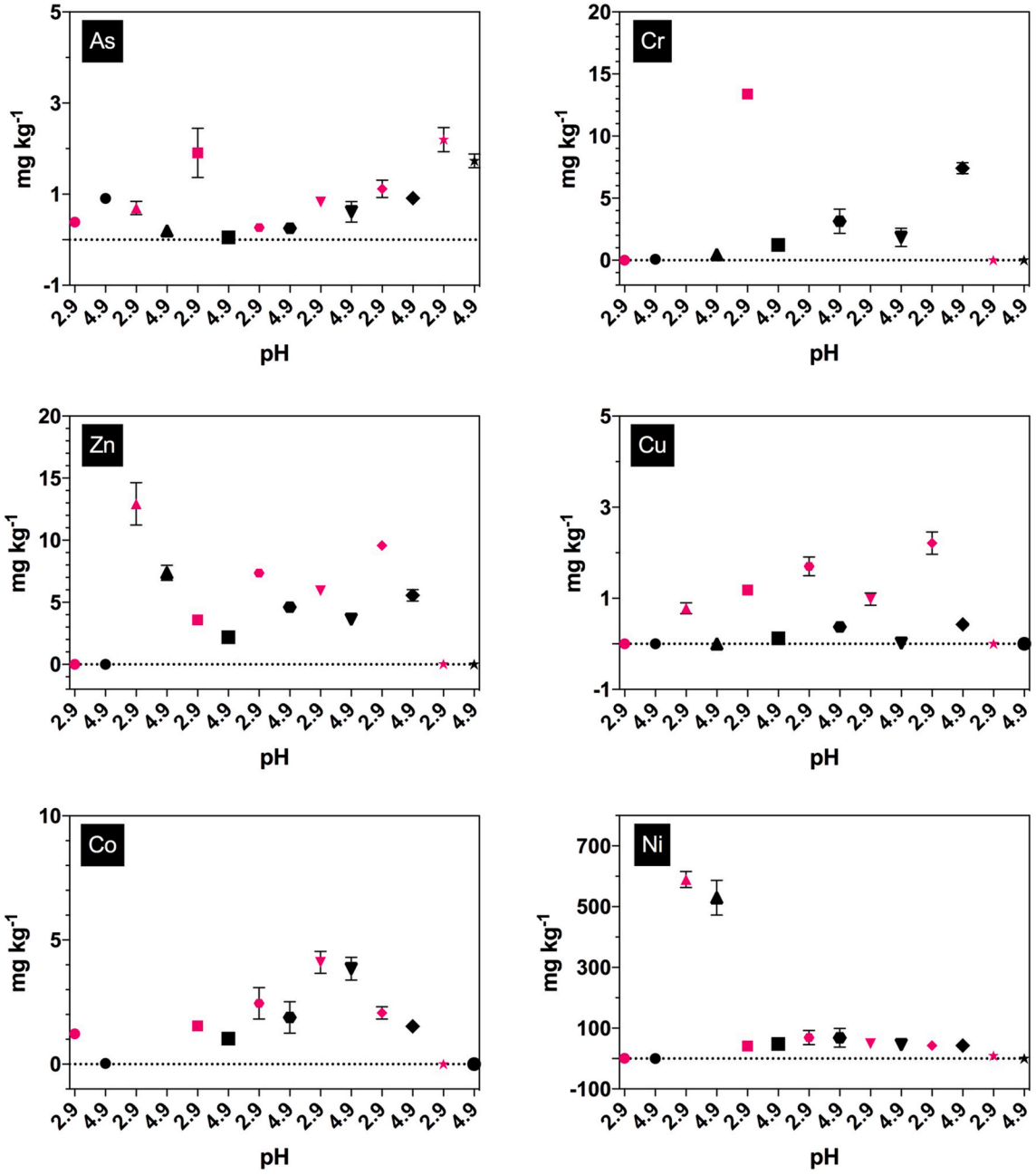

Fig. 7. Contaminants leaching from studied slags. Legend: circle (CS), triangle-up (IS A), square (RS), hexagon (ICS), triangle-down (IS C), quadrangle (IS B), star (MS). Standard limits for As and Cr (100 mg kg^{-1}). Points plotted as zero indicate values below the detection limits.

of Cr (Kimbrough et al., 1999). The Cr^{3+} predominates under acidic conditions and can be leached from chromites (individual ones of chromites and chromites as nanoparticles in silicates). Trivalent form of chromium can be oxidized to Cr^{6+} under alkaline conditions posing high environmental risk. The formation and leaching of Cr^{6+} is possible in our study since secondary calcite and Ca-hydroxides identified in slag samples are able to favor of formation of alkaline conditions. Nevertheless, the Cr^{6+} can be later reduced to less toxic Cr^{3+} under the influence of acidic solutions in field conditions (i.e., root exudates, low-pH rains). Furthermore, the reactions between Cr^{3+} and Cr^{6+} can be governed by other abiotic as well as biotic factors (Gorny et al., 2016). Presence of Mn-(hydr)oxides can favor oxidation of Cr^{3+}. In turn, biotic reduction of Cr^{6+} to Cr^{3+} can occur through either detoxification or dissimilatory reduction, whereas Mn-oxidizing bacteria favors Cr^{3+} oxidation (Gorny et al., 2016). Lead leaching was minimal and, in most cases, not detected in the studied leachates, most likely due to the low lead content of the studied slags (2.1–18.7 mg kg^{-1}). Arsenic leaching was far above the allowable limit; its leachability at low pH was up to 36 higher than that at pH 4.9. Furthermore, to compare the susceptibility of samples to leaching, the contaminants extraction expressed in mg per kg of sample was recalculated based on the initial content in slags to obtain the amount expressed in %. In terms of general sample solubility, it was determined that up to 3.9% Zn was released from IS A, nearly 100% Co was released from IS A, 80.2% Ni was released from ISA, 15.5% Cu was released from ISB, 84.4% As was released from MS, 0.5% Cr was released from IS B, 4.2% V was released from MS, and up to 1% Pb was released from IS A. These findings indicated that the ISA sample was the most susceptible to contamination leaching. As a result, this sample should be regarded as a slag of concern from an environmental standpoint, as severe weathering occurring in the disposal environment may result in a

significant input of contaminants. Different leaching behaviors of studied slags exposed to leaching suggested that different mineral phases and their structures, in combination with their different reactivities, account for variable leaching behavior under acidic (pH 2.9) and slightly acidic (pH 4.9) conditions, which is consistent with previous research (Engström et al., 2012; Strandkvist et al., 2015). Even though the studied slags were found to be low risk according to US EPA standards, their general susceptibility to release contaminants should not be overlooked in the long run. It should be noted that even under laboratory conditions, leaching is known to be faster than in the field (Piatak et al., 2015; Liu et al., 2018), and that continuous exposure of slags to weathering may result in phase dissolution and subsequent release of contaminants into the surrounding environment.

Despite the fact that FeNi slag is not hazardous, preventive measures such as stabilization and consolidation using appropriate binders and geomaterials must be taken when designing the reclamation to avoid future restrictions. Primary slag components (e.g. olivine, pyroxene, glass) as well as minor phases (e.g. sulfides and intermetallic phases) differ in dissolution susceptibility. Consequently, the rates achieved under defined experimental conditions differ from rates observed in the field environmental conditions, with the latter conditions affecting slags stability at slower rates.

5. Conclusion

In the slags from laterite Ni ore smelting from the smelter of Euronickel company, we characterized three groups of slags: (i) electric furnace slags (EFS) of different ages and different ores used for the smelting, (ii) converter slags (CS) of different ages and (iii) magnetic slags (MS). Among themselves, EFS differ slightly to significantly in their mineralogy and chemistry, in comparison to the CS and MS. Phase assemblages and phase compositions reflecting the bulk composition of the EFS are similar to those derived from smelting of sulfide ores and to the limited studies on the slags from the smelting of the lateritic Ni ores. Slags from Euronickel Industries contain significant amounts of PTEs: up to 3000 ppm Ni, 17500 ppm Cr, and 130 ppm Co. The metal-extraction processes led to the redistribution of some elements and produced new phases that concentrated metallic elements. Sulfides (pentlandite, heazlewoodite and pyrrhotite) and intermetallic compounds (from the pure Fe, over Fe_7Ni_3 to Ni_3Fe) are the most important PTE carriers in the Euronickel slags. Important amounts of PTE (especially Cr) occur also in spinel-group phases. Because silicates from industrial slags crystallize from a melt under conditions of high activity of certain elements, they can also be discreetly enriched in PTE. In the EFS slags of Euronickel Industries that is the case with slightly elevated amounts of Cr in olivine and pyroxene.

Standardized leaching tests TCLP carried out on seven group of samples of metallurgical slags demonstrated low risk of contamination when referred to US EPA norm. However, given the overall slag susceptibilities to release contaminants these materials should be considered as potentially risky in a long-term perspective.

More detailed investigations on the microbially-mediated weathering of the soils surrounding Euronickel smelter are currently under progress.

CRediT authorship contribution statement

Tamara Đorđević: Writing – review & editing, Writing – original draft, Methodology, Investigation, Formal analysis, Conceptualization. **Goran Tasev:** Writing – review & editing, Visualization, Project administration, Funding acquisition. **Claudia Aicher:** Investigation. **Anna Potysz:** Writing – review & editing, Investigation, Formal analysis. **Peter Nagl:** Investigation, Formal analysis. **Christian L. Lengauer:** Resources, Investigation, Funding acquisition. **Artur Pędziwiatr:** Investigation, Formal analysis. **Todor Serafimovski:** Resources, Funding acquisition. **Ivan Boev:** Investigation, Data curation. **Blažo Boev:** Validation, Supervision, Resources.

Declaration of competing interest

The authors declare that they have no known competing financial interests or personal relationships that could have appeared to influence the work reported in this paper.

Data availability

Data will be made available on request.

Acknowledgements

The Federal Ministry of Education, Science, and Research (Republic of Austria) and the Austrian Agency for Education and Internationalization (OeAD) as well as Macedonian Ministry of Education and Science (MON) have provided financial support for the Scientific and Technological Cooperation Program between North Macedonia and Austria 2022–2023 [grant number MK 06/2022]. We express our gratitude to Maja Pacheshkoska, Lefteris Kaklamanos, and Simon Temelkov of Euronickel Industries GmbH for providing us with an overview of the ferronickel production process and for making slag sampling possible. We express our gratitude to Dr. Uwe Kolitsch for his valuable assistance during some of the SEM-EDX measurements. We are thankful to Vojtěch Ettler for the editorial handling of the manuscript and to two anonymous reviewers for their careful corrections and comments, which helped to improve the manuscript. The authors acknowledge TU Wien Bibliothek for financial support through its Open Access Funding Programme.

Appendix A. Supplementary data

Supplementary data to this article can be found online at https://doi.org/10.1016/j.apgeochem.2024.106068.

References

Bačeva Andonovska, K., Stafilov, T., Karadjova, I., 2015. Assessment of trace elements bioavailability – ingestion of toxic elements from the attic dust collected from the vicinity of the ferro-nickel smelter plant. Contributions, Section of Natural, Mathematical and Biotechnical Sciences. MASA 36, 93–104.

Bačeva, K., Stafilov, T., Šajn, R., Tanaselia, C., 2012. Moss biomonitoring of air pollution with heavy metals in the vicinity of a ferronickel smelter plant. J. Environ. Sci. Health A 47, 645–656.

Boev, B., Bermanec, V., 2005. Phase composition of the slag of the Feni Industry metallurgical plant and its impact on the environment. In: Boev, B., Serafimovski, T. (Eds.), Proceedings of the 3rd International Workshop on the Project Anthropogenic Effects on the Human Environments in Tertiary Basins in the Mediterranean. Štip: Faculty of Mining and Geology, pp. 57–67.

Boev, I., Šijakova-Ivanova, T., Mirakovski, D., 2013. Scanning electron microprobe characterization of air filters from the Kavadarci town and Tikveš valley. Geol. Maced. 27, 13–24.

Bolaños-Benítez, V., van Hullebusch, E.D., Lens, P.N.L., Quantin, C., van de Vossenberg, J., Subramanian, S., Sivry, Y., 2018. (Bio)leaching behavior of chromite tailings. Minerals 8. https://doi.org/10.3390/min8060261.

Crundwell, F.K., Moats, M.S., Ramachandran, V., Robinson, T.G., Davenport, W.G., 2011. Extractive Metallurgy of Nickel, Cobalt and Platinum-Group Metals. Elsevier, Amsterdam.

Engström, F., Adolfsson, D., Samuelsson, C., Sandström, Å., Björkman, B., 2012. A study of the solubility of pure slag minerals. Mine Eng. 41, 46–52.

Ettler, V., Johan, Z., Kříbek, B., Šebek, O., Mihaljevič, M., 2009a. Mineralogy and environmental stability of slags from the Tsumeb smelter, Namibia. Appl. Geochem. 24, 1–15.

Ettler, V., Cervinka, R., Johan, Z., 2009b. Mineralogy of medieval slags from lead and silver smelting (Bohutín, Příbram district, Czech Republic): towards estimation of historical smelting conditions. Archaeometry 51, 987–1007. https://doi.org/10.1111/j.1475-4754.2008.00455.x.

Ettler, V., Kvapil, J., Šebek, O., Johan, Z., Mihaljevič, M., Ratié, G., Garnier, J., Quantin, C., 2016. Leaching behaviour of slag and fly ash from laterite nickel ore smelting (Niquelândia, Brazil). Appl. Geochem. 64, 118–127. https://doi.org/10.1016/j.apgeochem.2015.09.019.

Ettler, V., Polák, L., Mihaljevič, M., Ratié, G., Garnier, J., Quantin, C., 2018. Oral bioaccessibility of inorganic contaminants in waste dusts generated by laterite Ni ore smelting. Environ. Geochem. Health 40, 1699–1712.

Euronickel, 2021. From ore to ferronickel description of the technological process. Brochure by the EURONICKEL INDUSTRIES KAVADARCI – RN MACEDONIA 16.
Garnier, J., Quantin, C., Guimarães, E., Becquer, T., 2008. Can chromite weathering be a source of Cr in soils? Mineral. Mag. 72, 49–53. https://doi.org/10.1180/minmag.2008.072.1.49.
Gregurek, D., Melcher, F., Pavlov, V.A., Reimann, C., Stumpfl, E.F., 1999. Mineralogy and mineral chemistry of snow filter residues in the vicinity of the nickelcopper processing industry, Kola Peninsula, NW Russia. Mineral. Petrol. 65, 87–111.
Gorny, J., Billon, G., Noiriel, C., Dumoulin, D., Lesven, L., Madé, B., 2016. Chromium behavior in aquatic environments: a review. Environ. Rev. 24, 503–516. https://doi.org/10.1139/er-2016-0012.
Jarošíková, A., Ettler, V., Mihaljevič, M., Kříbek, B., Mapani, B., 2017. The pH-dependent leaching behavior of slags from various stages of a copper smelting process: environmental implications. J. Environ. Manag. 187, 178–186. https://doi.org/10.1016/j.jenvman.2016.11.037.
Kierczak, J., Néel, C., Puziewicz, J., Bril, H., 2009. The mineralogy and weathering of slag produced by the smelting of lateritic Ni ores, Szklary, Southwestern Poland. Can. Mineral. 47, 557–572. https://doi.org/10.3749/canmin.47.3.557.
Kierczak, J., Pietranik, A., 2011. Mineralogy and composition of historical Cu slags from the Rudawy Janowickie Mountains, southwestern Poland. Can. Mineral. 49 https://doi.org/10.3749/canmin.49.5.1281, 1281-1269.
Kierczak, J., Pietranik, A., Piatak, N.M., 2021. Weathering of slags. CHAPTER 4. 125–150. https://doi.org/10.1039/9781839164576-00125.
Kimbrough, D.E., Cohen, Y., Winer, A.M., Creelman, L., Mabuni, C., 1999. A critical assessment of chromium in the environment. Crit. Rev. Environ. Sci. Technol. 29, 1–46. https://doi.org/10.1080/10643389991259164.
Lanteigne, S., Schindler, M., McDonald, A.M., Skeries, K., Abdu, Y., Mantha, N.M., Murayama, M., Hawthorne, F.C., Hochella Jr., M.F., 2012. Mineralogy and weathering of smelter-derived spherical particles in soils: implications for the mobility of Ni and Cu in the surficial environment. Water, Air, Soil Pollut. 223, 3619–3641.
Lanteigne, S., Schindler, M., McDonald, A., 2014. Distribution of metals and metalloids in smelter-derived particulate matter in soils and mineralogical insights into their retention and release in a low-T environment. Can. Mineral. 52, 453–471.
Lastra, R., Carson, D., Koren, D., 1998. Mineralogical characterization of leachable elements in ten slags from Canadian non-ferrous sulphide smelters. In: Petruk, W. (Ed.), Waste Characterization and Treatment Symposium. SME, Lit-tleton, USA, pp. 79–90.
Li, Y., Papangelakis, V.G., Perederiy, I., 2009. High pressure oxidative acid leaching of nickel smelter slag: characterization of feed and residue. Hydrometallurgy 97, 185–193.
Liu, T., Li, F., Jun, Z., Yang, Y., 2018. Acidic leaching of potentially toxic metals cadmium, cobalt, chromium, copper, nickel, lead, and zinc from two Zn smelting slag materials incubated in an acidic soil. Environ. Pollut. 238, 259–368. https://doi.org/10.1016/j.envpol.2018.03.022.
Ljatifi, E., Grozdanov, A., Načevski, G., Paunović, P., 2014. Production of glass using metallurgical solid waste aimed for formation of glass-ceramic. 7th Expert counselling: Technology of underground and surface exploitation of mineral resources, PODEX – POVEX 14, 245–252.
Lottermoser, B.G., 2002. Mobilization of heavy metals from historical smelting slag dumps, north Queensland, Australia. Mineral. Mag. 475–490.
Miceva, O., Hristovski, S., Melovski, Lj, 2019. The impact of the ferro-nickel smelter's fugitive dust emission on heavy metal content in soils and Whitetop (Lepidium draba L.) in Kavadarci, Republic of Macedonia. Fresenius Environ. Bull. 28, 1189–1202.
Nagl, P., Mader, D., 2019. X-ray fluorescence (XRF) and instrumental neutron activation analysis (INAA) for the geochemical analysis of rocks, presented on in-house control samples. Mitt. Österr. Mineral. Ges. 165, 67.
Piatak, M.N., Parsons, M.B., Seal II, R.R., 2015. Characteristics and environmental aspects of slag: a review. Appl. Geochem. 57, 236–266.
Perederiy, I., Papangelakis, V.G., Buarzaiga, M., Mihaylov, I., 2011. Co-treatment of converter slag and pyrrhotite tailings via high pressure oxidative leaching. J. Hazard. Mater. 194, 399–406.. https://doi.org/10.1016/j.jhazmat.2011.08.012.
Piatak, M.N., Ettler, V., Hoppe, D., 2021. Geochemistry and mineralogy of slags. CHAPTER 3, 59–124. https://doi.org/10.1039/9781839164576-00059.
Ratié, G., Quantin, C., Jouvin, D., Calmels, D., Ettler, V., Sivry, Y., Cruz Vieira, L., Ponzevera, E., Garnier, J., 2016. Nickel isotope fractionation during laterite Ni ore smelting and refining: implications for tracing the sources of Ni in smelter-affected. Appl. Geochem. 64, 136–145. https://doi.org/10.1016/j.apgeochem.2015.09.005.
Saha, A.K., Sarker, P.K., 2016. Expansion due to alkali-silica reaction of ferronickel slag fine aggregate in OPC and blended cement mortars. Construct. Build. Mater. 123, 135–142.
Serafimovski, T., Volkov, A.V., Boev, B., Tasev, G., 2013. Ržanovo metamorphosed lateritic Fe–Ni deposit, Republic of Macedonia. Geol. Ore Deposits 55, 283–389.
Schindler, M., 2014. A mineralogical and geochemical study of slag from the historical O'Donnell Roast Yards, Sudbury, Ontario, Canada. Can. Mineral. 52, 433–452.
Swartzendruber, L.J., Itkin, V.P., Alcock, C.B., 1991. The Fe–Ni (iron-nickel) system. J. Phase Equil. 12, 288–312.
Spirovska, M., 2010. Environmental Impact Assessment Study from the Construction of a Slag Dump. DECONS-EMA. Environmental Consulting Company for FENI Industries, p. 96 (in Macedonian).
Strandkvist, I., Björkman, B., Engström, F., 2015. Synthesis and dissolution of slag minerals – a study of β-dicalcium silicate, pseudowollastonite and monticellite. Can. Mennon. Q. 54, 446–454.
US EPA, Office of solid waste (OSW), catalog of hazardous and solid waste, http://www.epa.gov/hw.
Vitkova, M., Ettler, V., Johan, Z., Kríbek, B., Sebek, O., Michaljevic, M., 2010. Primary and secondary phases in copper-cobalt smelting slags from the Copperbelt Province, Zambia. Mineral. Mag. 74, 581–600. https://doi.org/10.1180/minmag.2010.074.4.581.
Warchulski, R., 2016. Zn-Pb slag crystallization: evaluating temperature conditions on the basis of geothermometry. Eur. J. Mineral 28, 375–384. https://doi.org/10.1127/ejm/2015/0027-2496.
Warner, A.E.M., Díaz, C.M., Dalvi, A.D., Mackey, P.J., Tarasov, A.V., 2006. JOM world nonferrous smelter Survey, part III: nickel: laterite. J. Occup. Med. 58, 11–20.
Xi, B., Li, R., Zhao, X., Dang, Q., Zhang, D., Tan, W., 2018. Constraints and opportunities for the recycling of growing ferronickel slag in China. Resour. Conserv. Recycl. 139, 15–16.